Liberation of a pinned spiral wave by a single stimulus in excitable media

Marcel Hörning,[1,*] Akihiro Isomura,[1,2] Konstantin Agladze,[2] and Kenichi Yoshikawa[1,†]
[1]*Department of Physics, Graduate School of Science, Kyoto University, and Spatio-Temporal Project, ICORP JST, Kyoto 606-8502, Japan*
[2]*Institute for Integrated Cell-Material Sciences (iCeMS), Kyoto University, Kyoto, Japan*
(Received 29 October 2008; published 23 February 2009)

The unpinning of a spiral wave from an anatomic obstacle by the application of a single stimulus near the core of the rotating wave was studied experimentally in a cell culture of cardiomyocyte monolayers as well as by computer simulations. It is shown that, with suitable positioning and timing, a single stimulus is sufficient for the successful unpinning of a pinned spiral wave. Successful unpinning is achieved when two conditions are fulfilled: (1) The stimulus is delivered in the vulnerable window of the rotating wave, and (2) the stimulus is delivered in a spatial zone in proximity to the obstacle, where the shape of the zone is defined by the phase of the anchored spiral wave. Two different scenarios for successful unpinning are discussed, which are distinguished by the distance to the stimuli applied to the obstacle.

DOI: 10.1103/PhysRevE.79.026218 PACS number(s): 05.45.−a, 87.19.Hh, 87.18.Hf

I. INTRODUCTION

Excitable systems are found throughout nature, in heart muscle [1,2], retina [3], and cultures of the slime mold dictyostelium discoideum [4]. These systems often exhibit a phenomenon of rotating waves (also known as spiral waves, reentries, and vortices). The mechanisms for initiating and methods for controlling rotating waves have been studied extensively in various chemical and biological systems [5–9]. A major reason why rotating waves have attracted so much interest is their role in the transition to a chaotic state in the heart, which results in fibrillation and sudden death. Thus, it is important to know how to control rotating waves so that we can prevent or suppress them. A mechanism proposed by Winfree, called the "pinwheel experiment" [10], indicated the role of the vulnerability by emphasizing the timing and strength of a stimulus applied in the vulnerable window (VW) of a propagating wave. Further extended studies revealed the role of the electrical restitution, stimulation sequence, and cellular electrophysiological properties to cardiac reentries [11,12].

In many instances, reentry-related tachycardia can be successfully terminated by the application of external pacing [13,14]. As recently shown in an experimental model, pacing may lead to drifting of freely rotating spiral waves and their collision with a boundary [2]. However, it is still not clear how to force pinned spiral waves (waves attached to anatomical heterogeneities) to drift. Pumir *et al.* [15] showed numerically that electric field-induced wave emission from heterogeneities (WEH) in the heart can terminate rotational waves, where the number of pacing sites increases with the amplitude. Such scenarios have been theoretically and experimentally supported in recent studies [16–20]. Cysyk and Tung [18] showed that electric field-induced WEH can directly excite heterogeneities in cardiomyocyte monolayers, and unpin rotational waves.

The present paper describes a study to eliminate a spiral wave pinned to an obstacle by the application of a single stimulus near the obstacle. The results indicate that successful unpinning can be interpreted in terms of a vulnerable window (VW) effect, when an external stimulus is delivered near or on the obstacle. This stimulus produces a pair of spiral waves, one of which annihilates the attached rotating wave, while the other either reattaches to the obstacle or remains free, depending on the time and location of the stimulus. The present paper shows VW-based unpinning experimentally in cardiomyocyte tissue culture and in detail in computer simulations. To understand the underlying mechanisms, we studied the short-term history of wave patterns in two-dimensional excitable media by varying the stimulus position in the VW of a propagating wave. Numerical studies were performed using the simplified ionic model of Fenton and Karma [21]. We found that a stimulus delivered in different phases of the refractoriness of a propagating wave (conditioning wave) results not only in different shapes for the produced spiral pairs [22], but also leads to a situation where the path of the wave-tip trajectories of the produced spirals depends on the apex angle. A stimulus applied close to the absolute refractoriness leads to a narrow apex angle and the produced spiral pairs meander away from the direction of the conditioning wave. However, a stimulus applied close to the region of fully recovered medium leads to a wide apex angle, and the produced spiral waves meander in the same direction as the conditioning wave.

Two different scenarios of unpinning the rotational wave from the obstacle are discussed, depending on the position of the stimulus within the VW of the rotational wave. Although there have been previous studies on the unpinning of spiral waves [19,20,23–27], to the best of our knowledge this is the first systematic investigation of the role of the vulnerable window in the unpinning of a spiral wave with a single stimulus in two dimensions. The goal of our studies was to investigate experimentally and numerically the spatiotemporal dependence of a stimulus that unpins a pinned spiral wave. Although the present study does not provide a realistic immediate way for the application in the clinics, it creates a conceptual background for the development of new methods

*Corresponding author; FAX: +81-75-753-3779; marcel@chem.scphys.kyoto-u.ac.jp
†yoshikaw@scphys.kyoto-u.ac.jp

for termination of reentry-based arrhythmia. Future development on the visual mapping of heart activity would open the possibility toward the clinical application.

II. NUMERICAL MODEL

To simulate cardiac electrical dynamics, we used the simplified ionic model of Fenton and Karma [21]. Although the model does not explicitly describe the channel properties of myocyte cells, it reproduces fairly well the action potential among different animal cells. The successful application of this model to the qualitative behavior of excitable media has been previously shown to explain problems in cardiac tissue [28].

The model is based on three main currents through the membrane: The fast inward current J_{fi} and the slow inward and outward currents J_{si} and J_{so}, respectively. The basic equation for the membrane potential $\mathbf{V}$ is given by

$$\partial_t \mathbf{V} = \nabla \cdot (D \nabla \mathbf{V}) - J_{\mathrm{Ion}}(\mathbf{V};\mathbf{v};\mathbf{w})/C_m, \tag{1}$$

where C_m is the membrane capacity, D is the diffusion, $\mathbf{v}$ and $\mathbf{w}$ describe the gating variables and J_{Ion} is the sum of the three main currents. The membrane potential $\mathbf{V}$ and currents J_{fi}, J_{si}, and J_{so} are scaled by definition to the dimensionless variables $u \equiv (V - V_o)(V_{fi} - V_o)$ and $I \equiv J/[C_m(V_{fi} - V_o)]$, respectively, where V_{fi} is the Nernst potential of the fast inward current and V_o is the resting membrane potential. With the substitution $u_s = u - u_c$, the currents are given as

$$I_{fi} = -\frac{v}{\tau_d}\Theta(u_s)(1-u)(u_s), \tag{2}$$

$$I_{si} = \frac{u}{\tau_o}\Theta(-u_s) + \frac{1}{\tau_r}\Theta(u_s), \tag{3}$$

$$I_{so} = -\frac{w}{2\tau_{si}}\{1 + \tanh[k(u - u_c^{si})]\}, \tag{4}$$

where $\Theta(x)$ is the Heaviside step function and τ_d are defined as

$$\Theta(x) = \begin{cases} 1 & \text{if } x > 0 \\ 0 & \text{otherwise,} \end{cases} \tag{5}$$

and

$$\tau_d = C_m/g_{fi}, \tag{6}$$

respectively. The model equations are described as

$$\partial_t u = D \nabla \cdot (\nabla \mathbf{u}) - I_{fi}(u;v) - I_{si}(u;w) - I_{so}(u), \tag{7}$$

$$\partial_t v = \Theta(-u_s)(1-v)/\tau_v^-(u) - \Theta(u_s)v/\tau_v^+, \tag{8}$$

$$\partial_t w = \Theta(-u_s)(1-w)/\tau_w^- - \Theta(u_s)w/\tau_w^+, \tag{9}$$

with

$$\tau_v^-(u) = [\Theta(u - u_v)\tau_{v1}^- + \Theta(u_v - u)\tau_{v2}^-]. \tag{10}$$

The diffusion coefficient $D = 1 \times 10^{-3}$ cm^2/ms is a constant, since our cardiomyocyte monolayers have no rotational anisotropy, as described in the original model of Fenton and Karma [21]. The model equations are solved by an explicit fourth-order Runge-Kutta method. The time step and grid size are given by 0.01 ms and 0.03 cm, respectively. For all simulations, the parameter values are $\tau_v^+ = 3.33$, $\tau_{v1}^- = 1000.0$, $\tau_{v2}^- = 19.2$, $\tau_w^+ - = 667.0$, $\tau_w^- = 11.0$, $\tau_d = g_{fi}^{-1}$, $\tau_0 = 8.3$, $\tau_r = 50.0$, $\tau_{si} = 44.84$, $k = 10$, $u_c^{si} = 0.85$, $u_c = 0.13$, $u_v = 0.055$, and $g_{fi} = 2.47$, respectively. The Nernst and resting membrane potentials are given by $V_{fi} = +15$ mV and $V_o = -85$ mV, respectively. The stimulus was applied with a radius of 0.1 cm and a duration of stimulation of 1.1 ms by setting the local membrane potential to +15 mV. This set of parameter leads to a meandering tip trajectory, which is essential for the following investigation.

III. NUMERICAL RESULTS

To understand the mechanism that underlies the liberation of a pinned spiral wave via a single stimulus, we studied the effect of stimulation in different phases in the VW along the direction of wave propagating in two-dimensional excitable medium. To demonstrate the effect of the VW for a one-dimensional propagating wave, a stimulus in the refractoriness of a propagating (conditioning) wave was induced. The time delay between the front of the conditioning wave and the applied stimulus defines the stimulus time, T_s, and the stimulus distance, d_s. Depending on T_s and d_s, the stimulus leads to bidirectional block, bidirectional wave propagation or unidirectional wave propagation. The latter can be achieved by pacing in the VW. Bidirectional block is defined by absolute refractoriness (AR), where the stimulus fails to propagate [29–31]. Figure 1(a) shows a propagating wave marked to show the region of the VW and AR. The figure also shows the region of the resting state (RS), where the applied stimulus can propagate freely. Figures 1(b) and 1(c) show the effect of pacing in the RS and VW in the one-dimensional case, and demonstrate the spatiotemporal evolution of bidirectional and unidirectional wave propagation, respectively.

While two-dimensional excitable systems have the same underlying physics, additional effects must be taken into account when the stimulus is applied in the VW. As shown in Fig. 1(b), the stimulus fails to propagate toward the direction of the conditioning wave. Such propagation failure is also seen in two-dimensional media. However, stimulation in the VW leads to asymmetric inhibition of the propagating wave and creates a pair of spiral waves [11,12]. In the following sections we first discuss the relation of stimulus time and subsequent opening angle of the two produced meandering spirals at a planar propagating wave, and then discuss the effect of the wave-tip propagation at different stimulus positions in proximity of the obstacle leading to unpinning the anchored spiral. Two mechanism of unpinning are discussed, which are distinguished by the distance to the stimuli applied to the obstacle. We will refer to the two discussed scenarios in the following as first and second scenario. The parameter set of the chosen model leads to a meandering spiral-tip trajectorieness. Thus, pacing into the VW of a propagating wave leads to the origination of two meandering spirals. Fig-

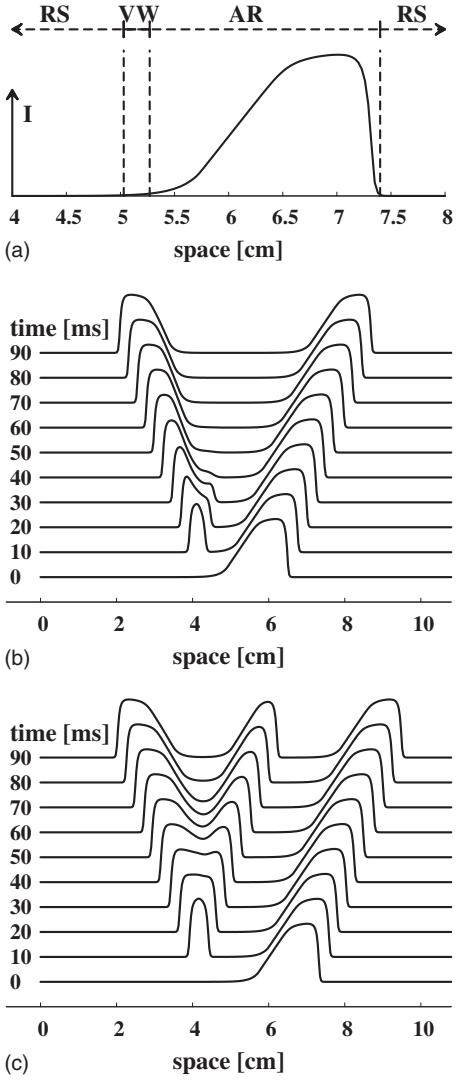

FIG. 1. Effect of the application of a single stimulus in a one-dimensional (1D) excitable system. (a) shows the intensity profile of a propagating wave, composed of three different states. The vulnerable window (VW), absolute refractoriness (AR), and resting state (RS) are indicated. (b) and (c) show the spatiotemporal profiles after the application of a stimulus in the RS and VW, respectively.

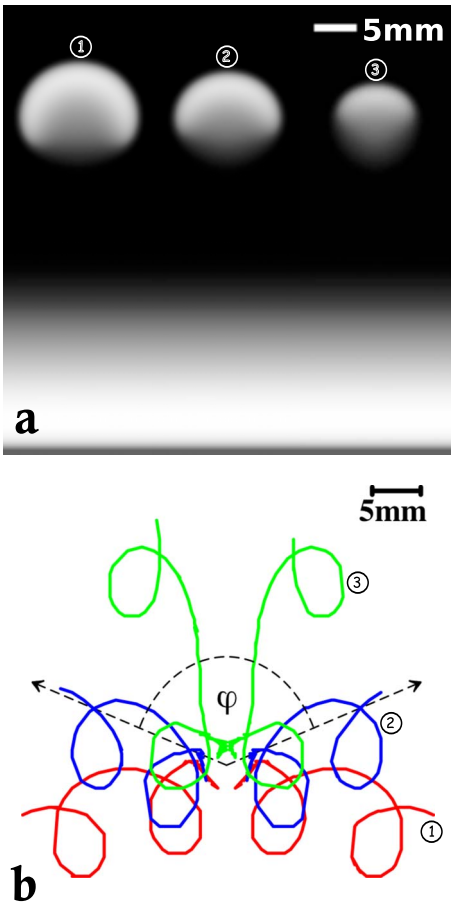

FIG. 2. (Color online) Appearance of a pair of spiral tips caused by a single stimulus with delay, T_s, after the propagation of a planar wave. (a) shows three independent stimuli applied in the VW of a downward-propagating wave. The image shows a snapshot at 36 ms after the stimulus was applied. The trajectories of the spiral pairs, tracked for 300 ms, are shown in (b). The applied stimuli correspond to T_s equal to 93 ms (red, 1), 91 ms (blue, 2), and 87 ms (green, 3). Smaller stimulation delays led to smaller apex angles of wave tip trajectories, and larger T_s led to larger apex angles. The apex angle φ is defined as the angle between the trajectories of the spiral pair, as sketched with black dashed lines.

ure 2(a) shows a snapshot of two independent stimuli applied with a delay of 40 ms to each other. The shape of the spiral pair is determined by T_s (the phase of stimulation) in the VW [22]. Stimulating into the VW close to the absolute refractoriness leads to a larger apex angle of the propagating wave than stimulation into the VW close to the fully recovered medium. This effect leads to trajectories of the produced spiral waves that depend on the stimulus position within the VW.

A. Propagation of spiral tips

To study the dependence of the trajectories of produced spiral pairs, we traced the tips of spiral pairs with stimuli applied at different T_s [see Fig. 2(b)]. To identify the spiral tip at each step, the intersection of a single isopotential line with a constant membrane potential, $V(r,t)=V_{\mathrm{iso}}$, where r is the position vector, and the point of zero normal velocity, $v(r,t)=0$, of each spiral were calculated and plotted at each time step. We chose the value of the isopotential line to be $V_{\mathrm{iso}}=-35$ mV, which represents the boundary between depolarized and repolarized regions of the media [21].

Figure 2 shows three different trajectories for the produced spiral pairs. Each pair of trajectories was obtained by stimulation at different phases (T_s) within the VW. The direction in which the trajectories are pointing is clear. If the stimulus is applied very close to the AR, the produced spiral waves annihilate each other after the first rotation and lead to circular wave propagation (not shown). This effect is seen only for a very small stimulation interval of approximately 1 ms for this particular excitability at $T_s \approx 87$ ms. Stimuli for slightly larger T_s lead, after the first rotation of the spiral waves, to long, straight meandering trajectories (green trajectory in Fig. 2). The spiral tips meander in the direction op-

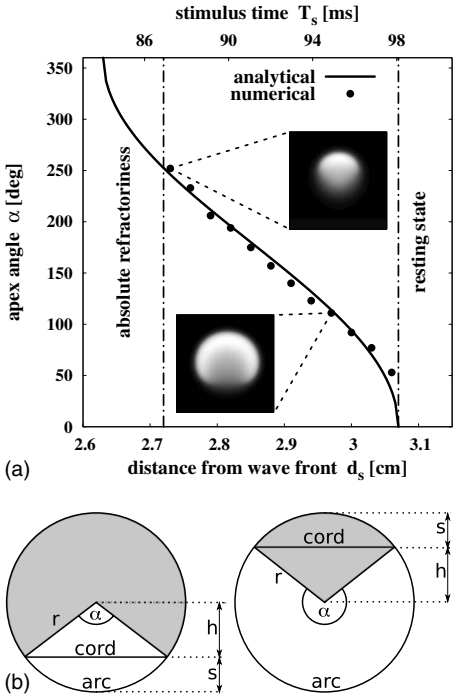

FIG. 3. Dependence of the apex angle of inhibition, α, on the stimulus time T_s and stimulus position d_s as illustrated by filled circles (a) Left and right vertical dotted-striped lines define the transient of the AR and RS regions. The analytical dependence [corresponding to Eq. (11)] is given by the solid black line, whereas the variables corresponding to α smaller and larger than 180°, respectively, are shown in (b).

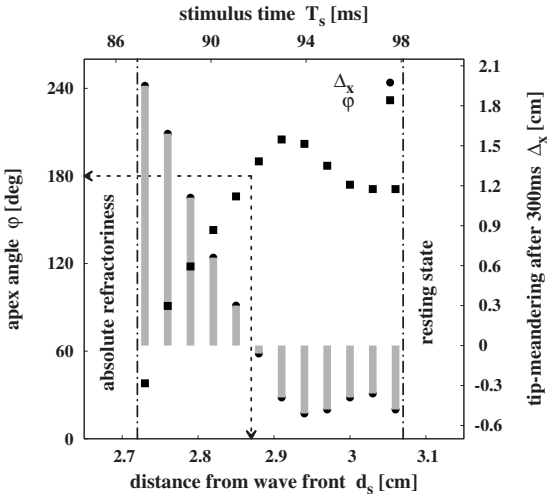

FIG. 4. Dependence of the apex angle of the paired trajectory, φ, and spiral-tip-displacement Δ_x after 300 ms with variation of the stimulus position in the VW. The angle φ is plotted with black squares corresponding to the left-hand axes. The spiral-tip-displacement is measured perpendicular to the conditioning wave after 300 ms of propagation, and is plotted with black filled circles highlighted by gray bars plotted from the origin of the applied stimulus. Left and right vertical dotted-striped lines define the transient of the AR and RS regions, which lead to inhibition of the stimulus and circular wave propagation, respectively. The striped arrows indicate the inflection point of displacement with respect to the conditioning wave.

posite the direction of propagation of the conditioning wave. However, the application of a stimulus for T_s larger than 92 ms leads to wave propagation of the spiral tip toward the direction of the conditioning wave (red trajectory in Fig. 2). The angle of the wave-tip trajectory can be defined by the apex angle φ between the trajectories of the spirals as exemplified by the blue trajectory in Fig. 2.

This phenomenon is caused by the different initial propagation of the applied stimuli. Stimulation closer to the AR leads to the inhibition of a larger area of the applied stimulus than a stimulus applied closer to the recovered region. This can be characterized by the apex angle of inhibition, α, where α is defined as the span of the annihilated region within the outward-propagating excited region. To clarify the geometrical dependence, α is illustrated in Fig. 3(b). Figure 3(a) shows the dependence of the stimulus time, T_s, of the propagating wave in the VW versus α with black points, and two representative examples are shown in insets. An analytical description is plotted as a black solid line, derived by the segment of a circle,

$$s(\alpha) = r - r\cos\left(\frac{\alpha}{2}\right), \tag{11}$$

where s is the distance from the midpoint of the chord to the midpoint of the arc, h is the distance from the midpoint of the chord to the center of the circle, r is the radius of the circle, and α is the apex angle of the inhibited area of the stimulus [see Fig. 3(b)]. This can be derived from the basic geometrical equations $h=r\cos(\frac{\alpha}{2})$ and $r=s+h$. The numerically obtained data of α show a good approximation to the analytical curve. Since the analytical expression is a pure geometrical approach, the solutions of α can also be found in the absolute refractoriness. If we consider only the dependence of the stimulus within the VW, a nearly linear dependence of α can be observed.

The apex angle, φ, the span of the trajectories produced by meandering of the spiral pairs [see Fig. 2(b)], leads to a more complex dependence, as illustrated in Fig. 4 with black squares. Additionally, the displacement, Δ_x, of the wave tips after 300 ms of propagation measured from where the stimulus was applied normal to the conditioning wave is shown as gray bars. The linear dependence of φ can be observed for stimuli applied near the AR. This trend changes to nonlinear dependence for stimuli applied close to the RS. The same linear and nonlinear dependence can be observed for displacement Δ_x for stimuli applied close to the AR and close to the RS, respectively. The inflection point of the direction of wave propagation is linked to φ equal to 180°, marked with black striped lines. The application of stimuli close to the AR led to small φ and large displacements in the direction opposite the conditioning wave, and the application of stimuli close to the RS led to large φ and small displacements toward the direction of propagation of the conditioning wave.

B. Unpinning via single stimulus

To take advantage of this effect, we numerically applied test stimuli around an obstacle-pinned spiral wave and ob-

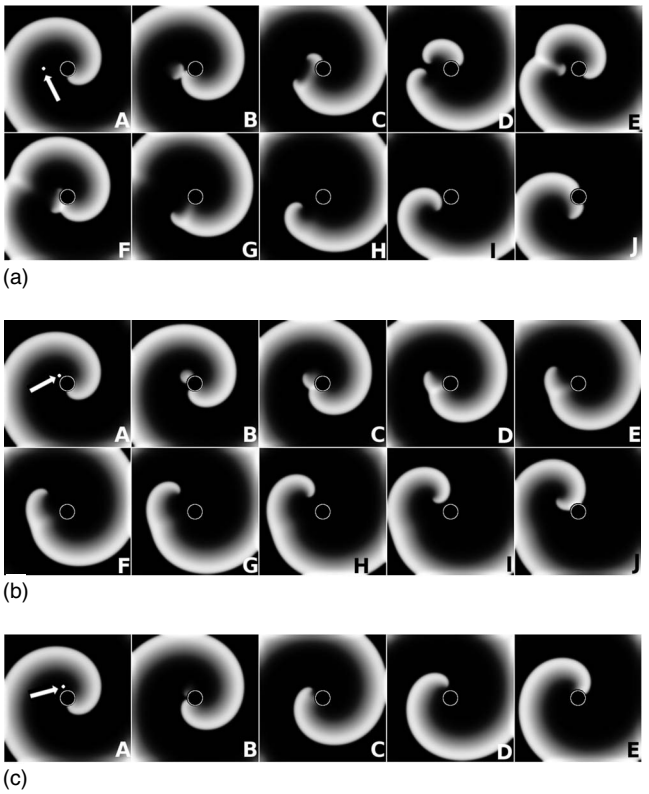

FIG. 5. Different scenarios after the application of a single stimulus near the obstacle pinned spiral wave. Field of view is 7.5 cm. Pacing locations are given in spherical coordinates with respect to the obstacle center and the pinned spiral wave front, respectively, and are shown by white filled circles and emphasized with white arrows in frame A. The obstacle has a radius of 0.5 cm. Frames are spaced every 30 ms. Three scenarios are shown: (a) Unpinning via the induction of a pair of spirals due to pacing into the VW of the rotating spiral apart from the obstacle. Pacing location is at (1.4 cm/270°). (b) Unpinning via pacing at the border on the obstacle. Pacing location is at (0.6 cm/225°). (c) Temporary unpinning of the spiral wave via pacing at the border of the obstacle. Pacing location is at (0.7 cm/200°).

served the effect on the formation of patterns in two dimensions (2D). We found different scenarios that led to the detachment of spiral waves by the application of a single stimulus near the obstacle. To simulate the obstacle, a circular area in the tissue was disconnected electronically by setting the diffusion constant to zero, corresponding to a nonflux boundary condition [9]. Figure 5 shows three different scenarios of detachment, and Fig. 5(c) only shows temporary detachment. Figure 5(a) shows unpinning via the creation of spiral pairs by the application of a single stimulus, which will be hereinafter referred to as first scenario. Frame A shows the position of the applied stimulus apart from the obstacle. The spiral tips propagate in a direction opposite the conditioning spiral arm (frame B), and annihilate the pinned spiral wave on the obstacle (frame C). The two free spiral arms rotate and annihilate each other, and the new gathered wave front propagates to the obstacle (frames D and E). The pinned spiral wave collides with the common wave front of the free spirals and the free spiral closer to the obstacle fails to propagate on the obstacle (frame F), so that only one spiral tip remains freely rotating apart from the obstacle (frames G–J). The second example of detachment is given in Fig. 5(b), and illustrates unpinning achieved by pacing on the obstacle border, which will be hereinafter referred to as second scenario. Frames A and B show excitation propagating from the stimulus applied to the obstacle border in the VW of the pinned spiral wave. Due to the disturbed propagation caused by the obstacle, one spiral tip develops freely next to the obstacle, whereas the other spiral tip propagates on the obstacle border and collides with the pinned spiral on the obstacle (frame C). The spiral arms on the obstacle annihilate each other and lead to a new merged wave front. The created free spiral of the applied stimulus becomes the new tip of the spiral wave (frames D–F). The new spiral wave propagates freely, as shown in frames G–J. The third scenario, shown in Fig. 5(c), illustrates the temporary detachment of the pinned spiral wave by the application of a single stimulus to the obstacle border. Frame A shows the stimulus applied to the border of the obstacle. Since the stimulus is applied in the AR of the pinned spiral wave, the stimulus fails to propagate (frame B), and leads to detachment of the pinned spiral wave (frames C and D). The pinned spiral wave reattaches to the obstacle (frame E) after propagation around the position at which the stimulus had been applied, since the excited area was not fully recovered until the spiral wave arrived.

We performed further numerical simulations to determine the probability of achieving unpinning of the spiral wave. Stimuli were isotropically distributed by varying the angle and the radius in steps of 15° and 0.2 cm, respectively. Figure 6 shows a map of stimuli that affect a pinned spiral wave. The initial pinned spiral is plotted in white as the corresponding color in the excitation map. Different stimulus positions are marked by different colors to classify the patterns to which the stimuli lead and are superimposed on the image of the pinned spiral wave. Each classified pattern is shown in Figs. 6(b)–6(d) and 6(f) by illustrating the propagating wave fronts with a time step of 5 ms for the first 75 ms after the stimulus was applied [32]. Green (cross) stimuli [Fig. 6(b)], are the stimuli applied to the absolute refractoriness of the spiral wave, and consequently they do not lead to wave propagation. Light-blue (plus-mark) stimuli [Fig. 6(c)] lead to wave propagation, but do not lead to the creation of spirals, and hence they do not influence the rotating spiral wave. While the blue (asterisk) stimuli [Fig. 6(d)] lead to the creation of spiral pairs, since they are applied to the VW of the pinned spiral wave, they do not lead to unpinning of the spiral wave. The produced spirals meander freely. The magenta (filled circle) [Fig. 6(e)] and yellow (square) stimuli [Fig. 6(f)] successfully unpin the pinned spiral wave from the obstacle. Corresponding examples are also shown in Figs. 5(a) (first scenario) and, 5(b) (second scenario), respectively. Both classes of stimuli are applied in the VW of the pinned spiral wave and lead to the creation of spiral tips. However, the scenarios are different, as explained above. The first scenario marked by magenta filled circles show exactly two spiral-pair rotations before the pinned spiral wave becomes unpinned. While blue (asterisk) stimuli applied closer to the obstacle do not lead to unpinning, it is more interesting that those applied in the VW close to the absolute

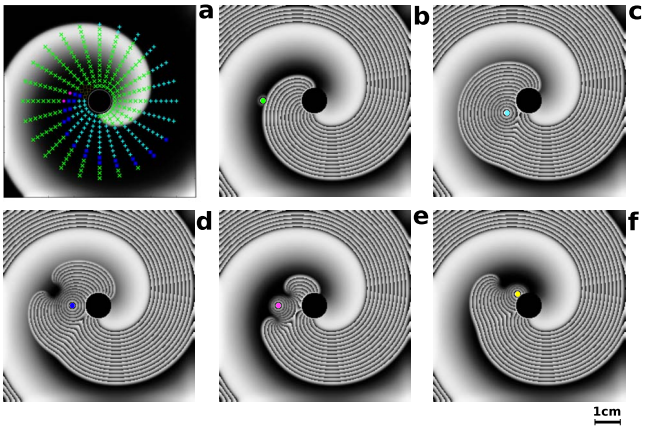

FIG. 6. (Color online) Map of stimuli that affect a pinned spiral wave. Field of view is 7.5 cm. The obstacle has a radius of 0.5 cm. (a) Stimuli are applied around the obstacle at steps of 15° and 0.2 cm in spherical coordinates. Different colors and symbols denote the formation of different patterns. (b)–(f) examplify the formation of each pattern, marked in the respective colors shown in (a). The initial pinned wave and the stimulus applied at $t=0$ ms are shown. In addition, the wave fronts of the propagating waves are shown with a step of 5 ms to illustrate the initial pattern formation up to $t=75$ ms. (b) Green (cross): Stimulus is applied in absolute refractoriness. No wave propagation is observed. (c) Light-blue (plus mark): Stimulus leads to circular wave propagation without affecting on the wave-tip trajectory of the pinned spiral wave. (d) Blue (asterisk): Creation of a free spiral, which does not lead to unpinning of the rotating wave. (e) Magenta (filled circle): Applied stimulus leads to spiral, pairs which in turn lead to unpinning of the spiral wave after the first rotation of their spiral tips. (f) Yellow (square): Applied stimulus leads to unpinning of the spiral wave immediately after stimulation.

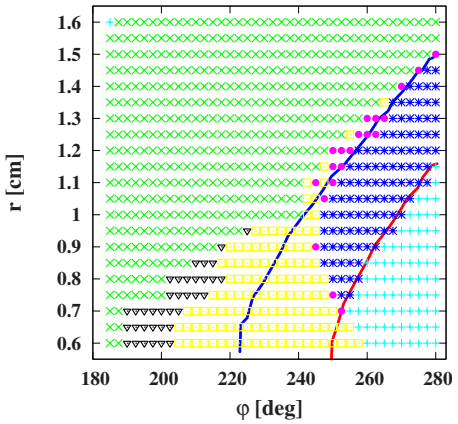

FIG. 7. (Color online) Close-up map of stimuli effects on a pinned spiral wave. The obstacle has a radius of 0.5 cm. Stimuli, shown in radial coordinates with r and ϕ, are applied in steps of 2.5° and 0.1 cm relative to the obstacle between 180° and 280°. The color coding corresponds to Fig. 6(a). Yellow (square): Applied stimulus leads to unpinning of the spiral wave immediately after stimulation; magenta (filled circle), applied stimulus leads to spiral pairs which lead to unpinning of the spiral wave after the first rotation of their spiral tips; light blue (plus mark), stimulus leads to circular wave propagation without affecting the tip trajectory of the pinned spiral wave; green (cross), stimulus is applied in the region of absolute refractoriness (no wave propagation). Black (triangle), applied stimuli lead to temporary detachment of the spiral wave; blue (asterisk), lead to spiral pairs which lead not to unpinning. The figure also shows two voltage isolines −84.9 mV and −84.7 mV in red (right-hand side) and blue (left-hand side), respectively.

refractoriness [close to the green (cross) stimuli] also lead to unpinning. This result can be easily explained by the effect discussed in the preceding section. Since the stimuli are applied close to the region of the AR, the stimuli lead to trajectories of the spiral tips with a small apex angle φ and large displacement in the direction opposite the conditioning wave. The spiral tips rotate toward the obstacle and lead to unpinning of the spiral. More details are provided in Sec. V.

The two scenarios shown in Fig. 5, as well as those shown in magenta (filled circle) and yellow (square) in Fig. 6, are limited to a small region near the obstacle, but are still very interesting. To analyze the region of interest, we performed more numerical simulations to achieve greater accuracy. We calculated pattern formation for applied stimuli in the obstacle range of 180° to 280°, with a step of 2.5°. The radius from the obstacle was from 0.6 cm to 1.6 cm with a step of 0.05 cm. The result is shown in Fig. 7. The polar coordinates ψ and r are plotted with respect to the obstacle center. Stimuli applied in the AR and in the region of the RS are indicated by light-blue plus signs and green crosses, respectively. Stimuli that lead to unpinning of the spiral without rotation of the produced spiral tips are marked by yellow squares, corresponding to the second scenario shown in Fig. 5(b) and the yellow squares in Fig. 6. Additionally, stimuli that lead to temporary unpinning are plotted as black triangles. An example is shown in Fig. 5(c). Furthermore, marks given in blue (asterisk) and magenta (filled circle) shown in the VW lead to wave breaks and subsequent anisotropic wave propagation. Stimulation at magenta (filled circle) marks (first scenario) leads to detachment of the spiral wave (see also the magenta filled circles in Fig. 6). This figure also shows isolines of voltage for the rotating spiral wave of −84.7 mV and −84.9 mV in red and blue, respectively. These two isolines mark the border of the VW of the pinned spiral wave. Magenta filled circles located on the blue higher-voltage isoline, as already explained above, lead to the first scenario of unpinning via meandering of the produced spiral pairs to the obstacle. However, this mechanism can also be found in the VW apart from the blue isoline, located between the region of produced spiral tips without consequent unpinning (blue asterisks) and the region of direct unpinning (yellow squares). This scenario can be found here as well, due to the nonlinear influence of the obstacle on the propagation of the produced spiral tips.

To understand our findings of the first scenario, two different trajectories of produced spiral pairs for successful and unsuccessful unpinning are shown in Figs. 8(a) and 8(b), respectively. The trajectories are superimposed on images of the applied stimulus and the pinned spiral wave. The meandering pathways of the spiral tips are presented in green (dashed line) and magenta (dotted line) to distinguish the pathways of the free spiral waves. In Fig. 8(a) the stimulus was applied close to the absolute refractoriness [comparable to the magenta (filled circle) marks in Fig. 6 and Fig. 7], leading to a small apex angle of tip trajectory, φ, meandering

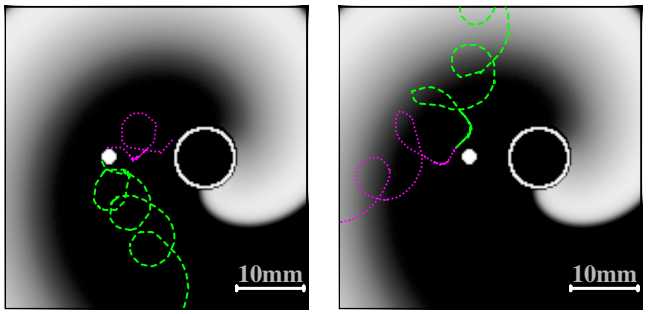

FIG. 8. (Color online) Close-up representation of successful (a) and unsuccessful (b) scenarios on which spiral tip trajectories convert a pinned spiral wave to an unpinned spiral wave with the application of a single stimulus. Trajectories of the spiral tips are shown as a green dashed line and magenta dotted line, respectively. The trajectories are superimposed on the initial applied stimulus and pinned rotating wave. Pacing locations are given in spherical coordinates with respect to the obstacle center and the pinned spiral wave front, respectively. (a) shows successful unpinning. Pacing location is at (1.4 cm/270°). The magenta dotted spiral tip failed to propagate on the obstacle. (b) shows successful unpinning. Pacing location is at (1.0 cm/270°). Spiral tips drift away from the obstacle, and do not lead to unpinning of the spiral wave.

in the direction to the obstacle. The upper magenta (dotted) trajectory collides with the obstacle after the first rotation and vanishes due to propagation failure. This example of unpinning corresponds to the example shown in Fig. 5(a). On the other hand, Fig. 8(b) shows an example in which the tips of both spiral arms drift away from the obstacle and do not lead to unpinning of the pinned spiral wave, since the stimulus was applied in the VW, but not sufficiently close to the region of the AR. No influence on the pinned spiral wave tip is observed, and the spiral wave remains pinned.

IV. EXPERIMENTAL RESULTS IN CARDIOMYOCYTE MONOLAYERS

For the experimental illustration of the unpinning scenario observed above in computer simulations, we performed observation on the tissue culture of cardiomyocytes. The example shown corresponds to the numerical examples shown in Figs. 5(a) and 8(a).

A. Experimental setup

Cell culture. Primary cell cultures of neonatal rat ventricular myocytes were prepared as described elsewhere [33]. Briefly, hearts isolated from neonatal Wistar rats of 1 day old were minced and treated with collagenase. The isolated cells were collected by centrifugation and preplated for 1 h. After the supernatant was collected again, the cells were plated on 22-mm-diameter glass coverslips coated with fibronectin (12 μg/ml) at a cell density of 2.6×10^3 cells/mm^2 with plating medium (Dulbecco-modified Eagle Medium with 10% fetal bovine serum, 1% penicillin streptomycin) and incubated for 24 hours in a humidified atmosphere at 37 °C and 5% CO_2. The medium was replaced by a contraction medium (minimum essential medium with 10% calf serum, 1% penicillin streptomycin) and the cells were incubated under the same conditions.

Observation. Experiments were performed 4–6 days after plating. Before each observation, the medium was replaced with Tyrode solution at room temperature, which includes 0.5 mM heptanol in order to decrease the wave speed. Cells were labeled with a Ca^{2+}-sensitive fluorescent dye, Fluo-4. Fluorescence was observed with an inverted microscope (IX-70; Olympus, Tokyo Japan) by the use of ×1.25 (PLAPON, N.A.=0.04; Olympus) low-magnification objective lens in combination with a ×0.35 intermediate lens [34]. Raw images were obtained with an electron multiplying CCD (iXon DV887ECS-UVB; Andor) with 128×128 pixels at a 14-bit resolution with 100 frames/s after 4×4 binning.

Electric stimulation of tissue was performed by the application of rectangular voltage pulses delivered by a pair of platinum electrodes. The anode was situated around the coverslip with a diameter of 5 cm and the cathode was placed above the stimulation point without touching the tissue, thus forming a monopolar stimulating electrode with a tip diameter of 0.5 mm. Spiral waves were initiated by high-frequency stimulation at the border of the tissue. In the core of a sustained spiral wave, the tissue was removed by a surgical procedure. The radius of the resulting obstacle was ca. 0.45 cm. The stimulating electrode was then placed above a point approximately 2.5 mm from the obstacle without touching the cell layer. At the core of the spiral wave, cells were surgically removed. We performed unpinning experiments only for a stable pinned spiral, which was confirmed to be sustained for more than 1 minute.

Data analysis. Data were processed by ImageJ [35] image-analysis software with custom plug-ins. The time series of each pixel was temporal low-pass filtered with a 5.0 Hz cutoff frequency for noise reduction and a Gaussian spatial convolution was applied with a radius of 2.0 pixels. Peak detection was performed and an activation time map was calculated [14,36].

B. Unpinning in cardiomyocyte monolayers

The spiral wave was produced and pinned to an obstacle as described above. Since it is difficult to produce a single stimulus precisely within the VW, stimulation was applied by periodic low-frequency stimuli of 1 Hz. Frequencies less than the rotational frequency of the pinned spiral are defined as low. This is a necessary condition to avoid the effect of unpinning via high-frequency pacing [13,14]. Figure 9 shows the temporary stable rotating waves leading the conversion of an obstacle-pinned spiral wave to a free spiral wave rotating separate from the obstacle. The successful induction of temporary stable spiral waves is shown in Fig. 9(a). The initiated wave propagates into the recovered region (blue area) in the direction of the obstacle, perpendicular to the pinned spiral wave, where the stimulus was applied in frame A. After annihilation of the merged wave front of the spiral pair with that of the pinned spiral, the free spirals continue to rotate (frames B and C) and lead to a new merged wave front (frames D and E). Due to the nonrecovered tissue, the wave

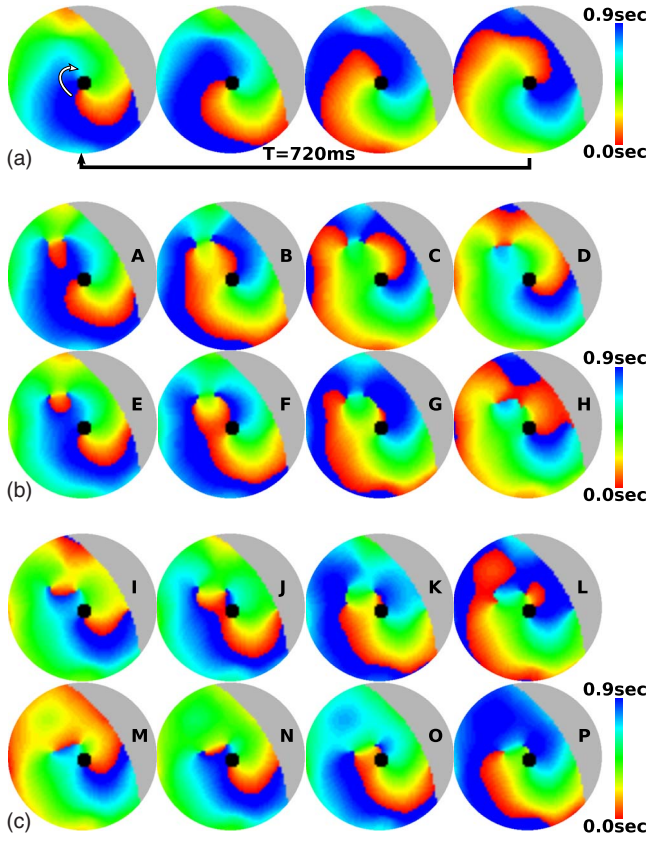

FIG. 9. (Color online) Experiment on a cardiomyocyte monolayer. Snapshots of successful unpinning via low-frequency pacing near the obstacle in cardiomyocyte monolayers. The pacing frequency and field of view are 1.0 Hz and 5 mm, respectively. The size of the obstacle is ~0.45 mm. Frames are spaced every 150 ms in (b) and (c). The unpinning scenario is divided into three parts: (a) Stable rotating spiral anchored at an obstacle with a period of rotation of 720 ms. The white arrow indicates the direction of rotation of the spiral; (b) creation of a spiral pair by the application of the stimulus in the VW of the pinned spiral wave apart from the obstacle; (c) successful unpinning by propagation failure of one spiral arm on the obstacle, and annihilation of the other free spiral wave with the pinned spiral wave.

must propagate within the recovered region (blue). The spiral tips propagate along a straight trajectory (frame F) before they continue to rotate (frames G and H). The newly formed wavelet, closer to the obstacle than the former one [see Fig. 9(b), frame I], annihilates the pinned spiral wave (frame J) again. Both free-rotating spirals continue to rotate (frame K). A second initiated wave propagates and annihilates the free-rotating spirals (frame L). The new merged wave front again annihilates the wave front of the pinned spiral wave. However, the wave front on the obstacle leads to a conduction block (propagation failure), as shown in frames N and O, so that the remaining free spiral becomes the new wave tip and is able to rotate freely approximately 2 mm from the obstacle (frame P). The free spiral remained stable at this position and did not drift to the border, as reported elsewhere [18], depending on the condition and size of the tissue.

Not every stimulus led to temporary stable spiral waves, where temporary stable waves are defined as free spiral waves that rotate more than one period. Temporary limited spiral waves, which are spiral waves that rotate only one time and lead to circular propagating waves, were observed for most of the applied stimuli (not shown). This effect was also observed in the numerical simulations, and will be discussed later. To obtain temporary stable spiral waves, stimulation must be applied in the VW close to the AR. This time window within the VW varies with the excitability of the medium [37], and can be very small.

V. DISCUSSION

In the present study, we demonstrated that it is possible to convert a pinned spiral wave to a free spiral wave by the application of only one stimulus in numerical simulations and by the application of low-frequency stimuli in cardiomyocyte monolayers. Two different scenarios of unpinning via the application of a single stimulus were observed in numerical simulations. In the first scenario, unpinning occurs via the creation of a pair of free spiral waves that meander to the obstacle and lead to unpinning of the pinned spiral wave, which was confirmed in experiments on cardiomyocyte monolayers. In the second scenario, unpinning was achieved via the application of stimuli in close proximity to the obstacle, which led to unpinning without rotation of the produced free spiral waves. Depending on the spatiotemporal application of the stimulus, temporary unpinning could also be observed. The unpinning of a pinned spiral wave from an anatomical obstacle by the production of spiral pairs apart from the obstacle will be discussed in more detail. In the numerical simulation, with the application of only a single stimulus, a pinned spiral wave could be converted to a freely rotating wave. However, in the experiment it was difficult to realize this scenario. The numerical simulations showed that stimulation only during a small time window within the VW led to successful unpinning. While the creation of free spiral waves is important, so is the stability and direction of propagation of the produced spiral waves, which are determined by the position of the stimulus applied in the VW. This limitation was also found in the experiments. Application of a single impulse as opposed to a high frequency pulse train would not have such negative consequences as tissue fatigue, and possible formation of new spiral waves due to the increasing functional inhomogeneity of the tissue. We thus regard the single-stimulus protocol as valuable, even if there exist difficulties toward the practical applicability at the present moment. To abolish this limitation on the dependency of the size of the VW, improved methods of optical mapping are needed. Alternatively, the active control of the size of time window of the VW can find a remedy, as shown in the previous studies [11,12]. Stimuli applied into the VW of a propagating wave in cardiomyocyte tissue led in most cases to the creation of temporary limited spiral pairs. Thus, after the first rotation of the produced spiral waves, the spiral arms collided to form a merged wave front, which led to circular wave propagation. Consequently, we changed the stimulation protocol from the application of a single stimulus to the application of low-frequency stimuli, and this led to a higher probability of obtaining stable free spiral waves. This

change led to the same effect of unpinning, since stimuli applied in the region of absolute refractoriness or stimuli that lead to temporary limited spiral waves have no influence on the subsequent stimulus. Therefore, it is important to use low-frequency pacing. Low frequency is defined as a frequency lower than the rotational frequency of the pinned spiral, where a stimulus does not effect a subsequent applied stimulus (defined by the restitution curve of the system). When the stimulation frequency is higher than that of the pinned spiral wave, pacing waves should approach the obstacle and might unpin the spiral wave. This mechanism of unpinning of a pinned spiral wave by high-frequency stimuli has been described in recent articles by Tanaka *et al.* [13] and Isomura *et al.* [14].

Despite the advantage of requiring only a single stimulus applied with low electrical current, which would cause no tissue damage, as in other procedures such as ablation or the use of defibrillators, other problems remain. Successful unpinning of a spiral wave does not necessarily include termination of the spiral wave from the tissue. Additional pacing protocols might be necessary to terminate the remaining free spiral wave. Cysyk and Tung [18] reported that converted free spiral waves drifted to the border of the tissue and self-terminated. However, this strongly depended on the tissue properties, such as the size and excitability of the tissue. Agladze *et al.* [2] demonstrated that stimuli applied with sufficiently high frequency led to the drift and eventual termination of a spiral wave at the border of the tissue. This procedure could be an important additional protocol for terminating the freely rotating unpinned spiral waves.

In both the numerical simulation and the experimental excitable system, unpinning of a pinned spiral wave with spiral pairs produced in the proximity of the obstacle was observed. However, the direction of propagation of the produced free spirals was determined by different factors. In the numerical simulation, the direction of the spiral tips was determined by the starting condition, whereas in cardiomyocyte tissue freely rotating waves always led to unpinning of a pinned spiral wave, even though only a few cases of unpinning could be observed experimentally. Due to the highly curved pinned spiral wave, the created spiral tips can only propagate in the direction of the obstacle, where the pinned spiral wave has its rotational origin, which consequently leads to unpinning. Figure 10 shows a snapshot of the propagating spiral pair leading to unpinning. An angle of approximately 60° points toward the vicinity of the obstacle and is indicated by two white, dashed arrows. The straight propagation toward the obstacle was measured to be approximately 1.1 mm. This relation between the angle and distance of propagation of the spiral wave supports the relation found in numerical simulations, where small angles lead to large displacement of the spiral tips. While not many cases of unpinning of spiral waves in cardiomyocytes have been observed, the production of spiral pairs near the obstacle always led to detachment of the pinned spiral wave. The development of precise stimulation protocols may increase the possibility of achieving unpinning of the spiral wave. Even a single well-directed stimulus might lead to wave detachment in cardiomyocyte tissue.

The present observation which are based on the application of a stimulus in the proximity of the obstacle can be explained by the effect of unpinning via WEH, as demonstrated in recent studies [15,18–20]. We applied stimuli through the use of monopolar point stimuli, whereas WEHs are based on the principle of far-field stimulation, which leads to depolarization on the obstacle. Despite the different stimulation protocols, the unpinning scenarios are based on comparable topologies. The effect of unpinning via the induction of WEH was observed experimentally by Cysyk and Tung [18]. If we compare their results to those we obtained in our numerical simulation, under the assumption that the systems are qualitatively comparable, we find similar values in both systems. Cysyk and Tung [18] observed experimentally that 33% of stimuli led to unpinning (termination) of the pinned spiral wave from an obstacle 2 mm in diameter. An unpinning rate of only 14% was observed for pinned spiral waves on obstacles of 3–4 mm in diameter. The stimuli were applied regardless of the phase of the pinned spiral wave, so that the data were obtained statistically. However, through the use of computer simulations we obtained a success rate of 15% for unpinning a spiral wave from a 1.0-mm-sized obstacle by stimulating on the border of the obstacle. This result was obtained by varying the position of the stimulus on the obstacle. By doubling the size of the obstacle, we could expect to approximately halve the probability that stimulation in the VW would lead to unpinning of a spiral wave. We confirmed this expectation by performing a numerical simulation and found that the success rate of unpinning a spiral wave from a 2-mm-sized obstacle fell to 7.2%. Even for systems that are not comparable with regards to excitability and the protocol for stimulation protocol, an increase in the size of the obstacle decreases the probability of unpinning a spiral wave by the application of a single stimulus on the obstacle. However, we should recall that the dependence on the applied current of the stimulus and its duration are also important. More detailed theoretical and numerical studies are necessary.

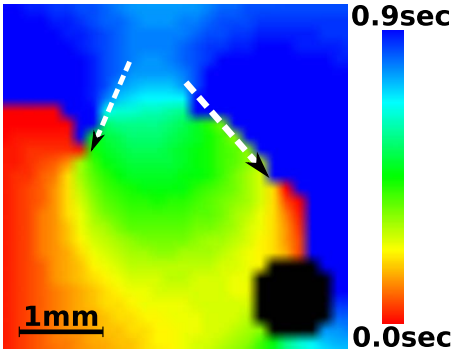

FIG. 10. (Color online) Close up of propagating wave tips in cardiomyocyte monolayer leading to unpinning of a pinned spiral wave. White dashed arrows correspond to the direction of propagation of the free spiral waves. The upper and lower tips of each line define the end and the start of rotation of the free spiral wave, respectively. The apex angle between both arrows is approximately 60 degrees, and the length of straight propagation (white dashed lines) is approximately 1 mm.

VI. CONCLUSION

Unpinning a pinned spiral wave with a single stimulus was studied using the numerical model of Fenton and Karma

[21] and an experimental model consisting of cardiomyocyte monolayers. In the present study, the spatiotemporal profile of a single stimulus applied to unpin the spiral wave was studied. The wave-stimulus dependence was systematically investigated in detail. Two mechanisms of unpinning, which depended on the spatiotemporal application of the stimulus, were observed and are explained here.

A numerical simulation was performed for a stimulus applied in the vulnerable window (VW) of a propagating wave. Stimuli applied in the VW lead to the creation of free rotational waves, whereas stimulation at different positions within the VW leads to different apex angles, φ, of the spiral tip trajectories. This effect is a main condition for observing the unpinning of a spiral wave. We found that stimuli applied in the VW close to the AR of a conditioning wave lead to wide φ, and thus the produced spiral wave propagates in the same direction as the conditioning wave. However, stimuli applied close to the RS lead to narrow φ and the spiral waves propagates in the direction opposite the conditioning wave. The inflection point for the direction of propagation is correlated to φ equal to 180°. With this effect, we demonstrated that two different unpinning scenarios exist caused by the application of a single stimulus into the VW, and these depend on the spatiotemporal position of the stimulus.

The first scenario is based on the application of a stimulus apart from the obstacle in the region of the VW of the pinned spiral wave. Stimuli applied in the VW close the RS of the pinned spiral wave to produce a pair of spirals, which propagate perpendicular to the obstacle and lead to unpinning of the pinned spiral caused by the propagation failure of one spiral arm on the obstacle and annihilation of the pinned spiral wave with the common wave front of the freely rotational spiral waves. This scenario of successful and unsuccessful unpinning was also observed in the actual experiments on cardiomyocyte monolayers. Since the position of the successful stimulus is restricted to a certain spatiotemporal range in the spiral arm, it is difficult to identify in cardiomyocyte monolayers. Thus, low-frequency stimulation was applied to increase the possibility of unpinning. While unpinning was observed in cardiomyocytes, the lack of accurate knowledge regarding the position and phase of the pinned spiral wave makes it difficult to observe unpinning. Further numerical and experimental studies are necessary to understand the generic behavior on the interesting phenomenon of unpinning via the application of single stimuli.

The second scenario is based on the application of a stimulus in the proximity of the obstacle in the region of the VW of the pinned spiral wave, which leads to unpinning of the pinned spiral wave. One of the produced spiral arms becomes pinned and propagates on the obstacle of the pinned spiral wave, whereas the other arm rotates freely next to the obstacle. The new pinned spiral arm collides with the pinned spiral wave and they merge to form a common wave front, so that the other produced freely rotating spiral becomes the new wave tip. Thus, the wave is unpinned from the obstacle. The probability of the application of a stimulus that leads to unpinning decreases with an increase in the size of the obstacle, consistent with the related experimental studies of Cysyk and Tung [18]. More studies are necessary to better understand the possibility of unpinning.

ACKNOWLEDGMENT

The authors would like to thank Dr. Valentin Krinsky (Max Planck Institute) for his helpful discussions.

[1] K. Nanthakumar *et al.*, Am. J. Physiol. Heart Circ. Physiol. **293**, 875 (2007).
[2] K. Agladze, M. Kay, V. Krinsky, and N. Sarvazyan, Am. J. Physiol. Heart Circ. Physiol. **293**, 503 (2007).
[3] M. Wiedemann, A. Piffel, and W. Hanke, Faraday Discuss. **120**, 237 (2001).
[4] F. Siegert and C. Weijer, Physica D **49**, 224 (1991).
[5] A. T. Winfree, Science **175**, 634 (1972).
[6] A. T. Winfree, Science **266**, 1003 (2004).
[7] J. Beaumont, N. Davidenko, J. Davidenko, and J. Jalife, Biophys. J. **75**, 1 (1998).
[8] D. Barkley, Phys. Rev. Lett. **72**, 164 (1994).
[9] Z. Qu, F. Xie, A. Garfinkel, and J. Weiss, Ann. Biomed. Eng. **28**, 755 (2000).
[10] A. T. Winfree, *The Geometry of Biological Time* (Springer, New York, 1980).
[11] M.-J. Yang, D. Tran, J. Weiss, A. Garfinkel, and Z. Qu, Am. J. Physiol. Heart Circ. Physiol. **293**, 1781 (2007).
[12] D. Tran, M. Yang, J. Weiss, A. Garfinkel, and Z. Qu, Chaos **17**, 043115 (2007).
[13] M. Tanaka, A. Isomura, M. Hörning, H. Kitahata, K. Agladze, and K. Yoshikawa (unpublished).
[14] A. Isomura, M. Hörning, K. Agladze, and K. Yoshikawa, Phys. Rev. E **78**, 066216 (2008).
[15] A. Pumir, V. Nikolski, M. Hörning, A. Isomura, K. Agladze, K. Yoshikawa, R. Gilmour, E. Bodenschatz, and V. Krinsky, Phys. Rev. Lett. **99**, 208101 (2007).
[16] E. Entcheva, J. Eason, I. Efimov, Y. Cheng, R. Malkin, and F. Claydon, J. Cardiovasc. Electrophysiol. **9**, 949 (1998).
[17] V. Fast, S. Rohr, A. Gillis, and A. Kléber, Circ. Res. **82**, 375 (1998).
[18] J. Cysyk and L. Tung, Biophys. J. **94**, 1533 (2008).
[19] S. Takagi, A. Pumir, D. Pazo, I. Efimov, V. Nikolski, and V. Krinski, J. Theor. Biol. **230**, 489 (2004).
[20] S. Takagi, A. Pumir, D. Pazo, I. Efimov, V. Nikolski, and V. Krinski, Phys. Rev. Lett. **93**, 058101 (2004).
[21] F. Fenton and A. Karma, Chaos **8**, 20 (1998).
[22] M. Gomez-Gesteira, G. Fernandez-Garcia, A. Munuzuri, V. Perez-Munuzuri, V. Krinsky, C. Starmer, and V. Perez-Villar, Physica D **76**, 359 (1994).
[23] L. Glass and M. E. Josephson, Phys. Rev. Lett. **75**, 2059 (1995).
[24] T. Nomura and L. Glass, Phys. Rev. E **53**, 6353 (1996).
[25] Y. Nagai, H. Gonzalez, A. Shrier, and L. Glass, Phys. Rev. Lett. **84**, 4248 (2000).
[26] S. Sinha and D. J. Christini, Phys. Rev. E **66**, 061903 (2002).

[27] P. Comtois and A. Vinet, Chaos **12**, 903 (2002).
[28] S.-J. Woo, J. Hong, T. Kim, B. W. Bae, and K. Lee, New J. Phys. **10**, 015005 (2008).
[29] F. Starmer, V. Biktashev, D. Romashko, M. Stepanov, O. Makarova, and V. Krinski, Biophys. J. **65**, 1775 (1993).
[30] C. Starmer, PACE **20**, 445 (1997).
[31] C. Starmer, Int. J. Bifurcation Chaos Appl. Sci. Eng. **12**, 1953 (2002).
[32] B. Forster, D. V. D. Ville, J. Berent, D. Sage, and M. Unser, Microsc. Res. Tech. **65**, 33 (2004).
[33] S. Matoba, T. Tetsuya, N. Keira, A. Kawahara, and K. Akashi, Circulation **99**, 817 (1999).
[34] E. Entcheva and H. Bien, Prog. Biophys. Mol. Biol. **92**, 232 (2006).
[35] W. Rasband, http://rsb.info.nih.gov/ij/
[36] S. M. Hwang, K. H. Yea, and K. J. Lee, Phys. Rev. Lett. **92**, 198103 (2004).
[37] A. Cimponeriu, C. Starmer, and A. Bezerianos, IEEE Trans. Biomed. Eng. **50**, 168 (2003).